Mechanochemical enzymes and protein machines as hydrodynamic force dipoles: The active dimer model

Yuto Hosaka* and Shigeyuki Komura†

Department of Chemistry, Graduate School of Science,
Tokyo Metropolitan University, Tokyo 192-0397, Japan

Alexander S. Mikhailov‡

Nano Life Science Institute (WPI-NanoLSI), Kanazawa University,
Kakuma-machi, Kanazawa, 920-1192, Japan and
Department of Physical Chemistry,
Fritz Haber Institute of the Max Planck Society,
Faradayweg 4-6, 14195 Berlin, Germany

Abstract. Mechanochemically active enzymes change their shapes within every turnover cycle. Therefore, they induce circulating flows in the solvent around them and behave as oscillating hydrodynamic force dipoles. Because of non-equilibrium fluctuating flows collectively generated by the enzymes, mixing in the solution and diffusion of passive particles within it are expected to get enhanced. Here, we investigate the intensity and statistical properties of such force dipoles in the minimal active dimer model of a mechanochemical enzyme. In the framework of this model, novel estimates for hydrodynamic collective effects in solution and in lipid bilayers under rapid rotational diffusion are derived, and available experimental and computational data is examined.

I. INTRODUCTION

Ligand-induced mechanochemical motions are typical for enzymes. Binding or dissociation of a ligand (i.e., substrate or product) to such proteins, as well as chemical reactions within the ligand-bound state, are often accompanied by conformational transitions in them. Thus, these macromolecules would repeatedly change their shapes in each next turnover cycle. The primary role of mechanochemical motions is to enable and facilitate catalytic reaction events. In the enzymes that operate as protein machines or molecular motors and catalytically convert ATP or GTP, such motions are moreover employed to bring about the required machine function or to generate work.

Since enzymes are in solution, their active conformational changes are accompanied by flows in the fluid around them. Such non-equilibrium flows can affect internal mechanical motions in the enzymes and also influence translational and rotational diffusion of such proteins, as demonstrated by MD simulations for a model protein [1] and adenylate kinase [2]. It has been discussed whether hydrodynamic self-propulsion of enzymes could furthermore occur, in the models where either instantaneous transitions [3, 4] or ligand-induced continuous conformational motions take place [5–7].

Lipid bilayers, forming biological membranes, behave as two-dimensional (2D) fluids on submicrometer scales [8, 9]. Biomembranes often include many active protein inclusions, such as ion pumps or transporters. Essentially, they represent protein machines powered by ATP hydrolysis or other catalytic reactions in them. Within each operation cycle, the shapes of their membrane domains typically change, inducing 2D fluid flows in the lipid bilayer around them [10]. As a result, active protein inclusions might even propel themselves through biomembranes [11].

Collective conformational activity of enzymes and protein machines leads to the development of non-thermal fluctuating flows in solution or a lipid bilayer. Other particles (i.e., passive tracers) are advected by these non-equilibrium flows, and, as previously shown [12], increased mixing in such systems and diffusion enhancement should therefore arise. Additionally, chemotaxis-like effects in the presence of spatial gradients in the concentration or the activity of enzymes can take place [12]. Remarkably, such phenomena persist even if mechanochemical motions are reciprocal; they do not rely on the presence of self-propulsion for proteins, which is predicted to be weak [5–7].

Following the original publication [12], extensive further research has been performed [13–20]. The effects of rotational diffusion and of possible nematic ordering for enzymes were considered [14], the phenomena in biomembranes were extensively analyzed [15, 16], and the theory was extended to viscoelastic media as well [17, 18]. Recently, it was shown that viscosity in dilute solutions of mechanochemically active enzymes should become also reduced [19]. Multiparticle numerical simulations of active oscillatory colloids, explicitly including hydrodynamic effects, were furthermore undertaken and principal theoretical predictions could thus be verified [20].

* hosaka-yuto@ed.tmu.ac.jp
† Corresponding author: komura@tmu.ac.jp
‡ mikhailov@staff.kanazawa-u.ac.jp

At low Reynolds numbers, the flow distribution produced by an object, changing the shape due to internal forces within it, can be characterized in the far field as that corresponding to a hydrodynamical force dipole. If the time-dependent stochastic force dipole of an enzyme is known, the collective hydrodynamic effects in solution of such enzymes are predicted by the mean-field theory [12]. The difficulty, however, is that experimental measurements and precise theoretical estimates for intensities and statistical properties of the force dipoles corresponding to actual enzymes are not available yet. Lacking this knowledge, only rough quantitative estimates for the considered collective hydrodynamic effects could be made so far.

The aim of the present study is to theoretically investigate hydrodynamic force dipoles in the simple active dimer model of an enzyme. The active dimer represents a minimal model where ligand-induced mechanochemical motions are reproduced [12, 20, 21]. The dimer consists of two beads connected by an elastic spring whose natural length depends on the ligand state. Under persistent ligand turnover, the dimer behaves like a mechanical oscillator and, within a fluid, plays a role of an oscillating force dipole. Large-scale numerical simulations of non-equilibrium colloids formed by such active dimers, with hydrodynamic effects fully taken into account in the multiparticle collision dynamics approximation [22], have been earlier performed; they could directly demonstrate the diffusion enhancement in such systems [20]. The relationship between this simple model and actual enzymes has been previously discussed [23].

In the next section, the active dimer model is formulated and its important statistical properties are introduced. After that, we undertake an approximate analytical investigation of statistical properties of the force dipoles corresponding to active dimers in Sec. III, followed by a numerical study in Sec. IV. Implications of our results for hydrodynamical diffusion enhancement effects in water solutions and in lipid bilayers are then considered in Secs. V and VI, respectively. Based on the new results, available experimental and computational data is examined in Secs. VII and VIII. The paper ends with the discussion of the obtained results.

II.   THE ACTIVE DIMER MODEL

The simplest mechanical system that gives rise to a hydrodynamic force dipole is a dimer. It consists of two beads 1 and 2 interacting via a potential $u(r)$ that depends on the distance $r = |\boldsymbol{r}_1 - \boldsymbol{r}_2|$ between them. The forces acting on the particles are $\boldsymbol{f}_1 = -\partial u/\partial \boldsymbol{r}_1 = \boldsymbol{f}$ and $\boldsymbol{f}_2 = -\boldsymbol{f}$. If the dimer is immersed into a viscous fluid, the velocity $\boldsymbol{V}$ of the hydrodynamic flow far enough from the dimer is approximately given by [12]

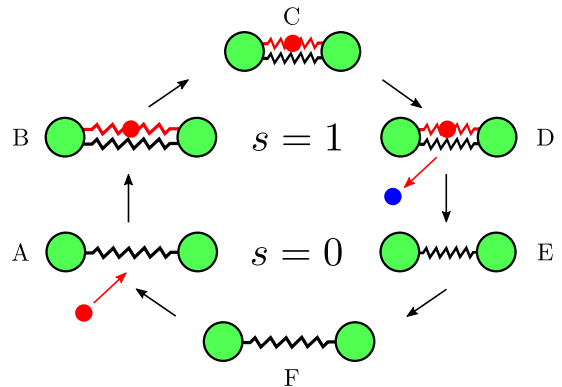$$V_\alpha = \frac{\partial G_{\alpha\beta}}{\partial R_\gamma} e_\beta e_\gamma m, \qquad (1)$$

FIG. 1. (Color online) The turnover cycle and mechanochemical motions in the active dimer model of an enzyme (see the text).

where $G_{\alpha\beta}(\boldsymbol{R})$ is the mobility tensor depending on the position $\boldsymbol{R}$ of the dimer with respect to the observation point, $\boldsymbol{e} = (\boldsymbol{r}_1 - \boldsymbol{r}_2)/r$ is the unit orientation vector of the dimer, and $m = fr$ is the magnitude of the force dipole. Summation over repeated indices is assumed. The force dipole is present only if there are non-vanishing net interaction forces, i.e., if the distance between the particles in a dimer continues to change.

The minimal active dimer model has been proposed [12, 21] (see also review [23]) to imitate mechanochemical conformational motions accompanying a catalytic turnover cycle in an enzyme. Its operation mechanism is illustrated in Fig. 1.

Two identical beads (green) are connected by an elastic link with a certain natural spring length ℓ_0 and stiffness k_0. A substrate particle (red) arrives (A) and binds as a ligand to the dimer by forming an additional elastic link with stiffness κ that connects the two beads (B). The natural length ℓ_c of this additional link is taken to be shorter than ℓ_0. Therefore, it tends to contract the dimer until a new equilibrium conformation (C) with a certain distance ℓ_1 between the beads is reached. Once this has taken place, a chemical reaction, that converts the ligand from the substrate to the product, occurs and the product (blue) is instantaneously released (D). Following the product release, the dimer is in the state E with the spring length ℓ_1 that is shorter than the natural length ℓ_0. Therefore, the spring expands and the domains move apart until the equilibrium state (F) is approached again. After that, a new substrate can bind, repeating the turnover cycle.

It is assumed that products are immediately evacuated and therefore we do not consider reverse product binding events. Moreover, possible dissociation events for the substrate are neglected assuming that its affinity is high.

Note that, since the product is immediately released once it has been formed, the ligand inside our model enzyme is always only in the substrate form. Therefore, the dimer can be either in the ligand-free ($s = 0$) or the ligand-bound ($s = 1$) states.

The elastic energies in these two states are

$$E_0(x) = \frac{k_0}{2}(x - \ell_0)^2, \tag{2}$$

and

$$E_1(x) = \frac{k_0}{2}(x - \ell_0)^2 + \frac{\kappa}{2}(x - \ell_c)^2 = A + \frac{k_1}{2}(x - \ell_1)^2, \tag{3}$$

where

$$A = \frac{\kappa k_0}{2(k_0 + \kappa)}(\ell_0 - \ell_c)^2, \qquad k_1 = k_0 + \kappa,$$
$$\ell_1 = \frac{k_0 \ell_0 + \kappa \ell_c}{k_0 + \kappa}, \tag{4}$$

and x is the distance between the beads.

The overdamped dynamics of the dimer in the ligand state s is described by the Langevin equation

$$\frac{dx}{dt} = -\gamma \frac{\partial E_s}{\partial x} + \xi(t), \tag{5}$$

where γ is the mobility coefficient. To account for thermal fluctuations, this equation includes thermal noise,

$$\langle \xi(t_1)\xi(t_2)\rangle = 2\gamma k_B T \delta(t_1 - t_2), \tag{6}$$

where k_B is the Boltzmann constant and T is the temperature.

Stochastic transitions between the two ligand states take place at constant rates v_0 and v_1 within narrow windows of width ρ near $x = \ell_0$ and $x = \ell_1$. If probability distributions $p_s(x,t)$ are introduced, they obey a system of two coupled Fokker-Planck equations

$$\frac{\partial p_0}{\partial t} = \frac{\partial}{\partial x}[\gamma k_0(x - \ell_0)p_0] + \gamma k_B T \frac{\partial^2 p_0}{\partial x^2} + u_1(x)p_1(x) - u_0(x)p_0(x), \tag{7}$$

and

$$\frac{\partial p_1}{\partial t} = \frac{\partial}{\partial x}[\gamma k_1(x - \ell_1)p_1] + \gamma k_B T \frac{\partial^2 p_1}{\partial x^2} + u_0(x)p_0(x) - u_1(x)p_1(x), \tag{8}$$

where $u_0(x) = v_0$ for $\ell_0 - \rho < x < \ell_0 + \rho$ and vanishes outside of this interval; $u_1(x) = v_1$ for $\ell_1 - \rho < x < \ell_1 + \rho$ and zero outside the interval. Note that the rate v_0 of substrate binding is proportional to the substrate concentration.

If the transition windows are very narrow, i.e., $\rho \ll \ell_0$ and $\rho \ll \ell_1$, one can use the approximation

$$u_0(x) = \nu_0 \delta(x - \ell_0), \qquad u_1(x) = \nu_1 \delta(x - \ell_1), \tag{9}$$

where $\nu_0 = 2v_0\rho$ and $\nu_1 = 2v_1\rho$.

Figure 2 shows the energy diagram of the model. Within each cycle, the dimer dissipates in mechanochemical motions the energy $\Delta E = \Delta E_0 + \Delta E_1$ which is furthermore equal to the difference $E_{sub} - E_{prod}$ of the energy $E_{sub} = E_1(\ell_0) - E_0(\ell_0)$ supplied with the substrate

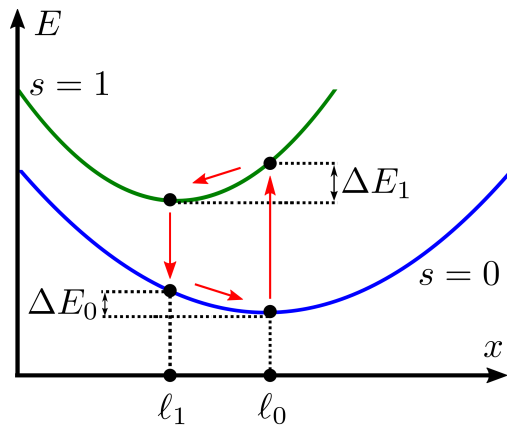
FIG. 2. (Color online) The energy diagram of the active dimer.

and the energy $E_{prod} = E_1(\ell_1) - E_0(\ell_1)$ removed with the product. We have

$$\Delta E = \frac{1}{2}(k_0 + k_1)(\ell_0 - \ell_1)^2. \tag{10}$$

The hydrodynamic force dipole of the active dimer is $m = k_0(\ell_0 - x)x$ for $s = 0$ and $m = k_1(\ell_1 - x)x$ for $s = 1$. Note that therefore $m \leq k_0 \ell_0^2/4$ for $s = 0$ and $m \leq k_1 \ell_1^2/4$ for $s = 1$.

When the transition windows are narrow, the probability rate w_0 that substrate binding, i.e., a transition to state $s = 1$, occurs per unit time in the state $s = 0$ is approximately

$$w_0 = \nu_0 \sqrt{\frac{k_0}{2\pi k_B T}}. \tag{11}$$

On the other hand, the probability rate w_1 that product release, i.e., a transition to state $s = 0$, occurs per unit time in the state $s = 1$ is then approximately given by

$$w_1 = \nu_1 \sqrt{\frac{k_1}{2\pi k_B T}}. \tag{12}$$

These equations are derived in Appendix A.

Moreover, the characteristic relaxation times of the dimer in the states $s = 0$ and $s = 1$ are, respectively, $\tau_0 = (\gamma k_0)^{-1}$ and $\tau_1 = (\gamma k_1)^{-1}$.

The parameter combinations $w_0\tau_0$ and $w_1\tau_1$ play an important role in determining the kinetic regimes. If the condition $w_0\tau_0 \ll 1$ is satisfied, equilibration to thermal distribution in the state $s = 0$ usually takes place before a transition to the state $s = 1$, i.e., binding of a substrate, occurs. If the opposite condition $w_0\tau_0 \gg 1$ holds, such transition takes place immediately after the transition window at $x = \ell_0$ is reached. If $w_1\tau_1 \ll 1$, the equilibration takes place in the state $s = 1$ before a transition to the state $s = 0$, i.e., the reaction and the product release, occurs. In the opposite limit with $w_1\tau_1 \gg 1$, the reaction takes place and product becomes released immediately once the respective window at $x = \ell_1$ is reached.

Note that, because the rate w_0 is proportional to substrate concentration, the condition $w_0\tau_0 \gg 1$ corresponds to the substrate saturation regime for the considered model enzyme. The condition $w_1\tau_1 \ll 1$ implies that the enzyme waits a long time before the product is released.

III. APPROXIMATE ANALYTICAL RESULTS FOR FORCE DIPOLES

At thermal equilibrium in the absence of substrate, $p_1(x) = 0$ and

$$p_0(x) = \sqrt{\frac{k_0}{2\pi k_B T}} \exp\left[-\frac{k_0}{2k_B T}(x - \ell_0)^2\right]. \tag{13}$$

Since $m = k_0(\ell_0 - x)x$, one can easily find the equilibrium statistical distribution for force dipoles by using the condition $P_{eq}(m)dm = p_0(x)dx$. Using, for convenience, the dimensionless force dipole magnitude $\widetilde{m} = m/k_0\ell_0^2$ and dimensionless temperature $\theta = k_B T/k_0\ell_0^2$, we get

$$P_{eq}(\widetilde{m}) = \frac{1}{\sqrt{2\pi(1 - 4\widetilde{m})\theta}}\left\{\exp\left[-\frac{1}{8\theta}(1 + \sqrt{1 - 4\widetilde{m}})^2\right]\right.$$
$$\left. + \exp\left[-\frac{1}{8\theta}(1 - \sqrt{1 - 4\widetilde{m}})^2\right]\right\}. \tag{14}$$

If $\theta \ll 1$, this distribution is approximately Gaussian and localized at $m = 0$, i.e.,

$$P_{eq}(\widetilde{m}) = \frac{1}{\sqrt{2\pi\theta}}\exp\left(-\frac{\widetilde{m}^2}{2\theta}\right). \tag{15}$$

Using the distribution (14), one finds that the mean force dipole is

$$\langle m \rangle_{eq} = -k_B T. \tag{16}$$

The correlation function $C(t) = \langle\Delta m(t)\Delta m(0)\rangle$ for variations $\Delta m = m - \langle m \rangle$ of force dipoles is [20]

$$C_{eq}(t) = k_0\ell_0^2 k_B T e^{-|t|/\tau_0} + 2(k_B T)^2 e^{-2|t|/\tau_0}, \tag{17}$$

where $\tau_0 = (\gamma k_0)^{-1}$ is the characteristic relaxation time for the dimer in the state $s = 0$.

As shown in Appendix B, the relation $\langle m \rangle = -k_B T$ is general and holds for the active dimer in any statistically stationary state.

When the dimer is catalytically active, four characteristic limits can be discussed.

A. The limit of $w_0\tau_0 \ll 1$ and $w_1\tau_1 \ll 1$

If the conditions $w_0\tau_0 \ll 1$ and $w_1\tau_1 \ll 1$ are both satisfied, binding of the substrate and product release have large waiting times.

In this regime, there are two almost independent equilibrium subpopulations of dimers in the states $s = 0$ and

$s = 1$. The relative weights of the subpopulations are $w_1/(w_1 + w_0)$ and $w_0/(w_1 + w_0)$. Therefore, all statistical properties are given by the sums of contributions from different states taken with the respective weights. Particularly, the correlation function of force dipoles is

$$C(t) = \frac{w_1}{w_0 + w_1}\left[k_0\ell_0^2 k_B T e^{-|t|/\tau_0} + 2(k_B T)^2 e^{-2|t|/\tau_0}\right]$$
$$+ \frac{w_0}{w_0 + w_1}\left[k_1\ell_1^2 k_B T e^{-|t|/\tau_1} + 2(k_B T)^2 e^{-2|t|/\tau_1}\right]. \tag{18}$$

We can use the above equation to determine the non-equilibrium part of the fluctuation intensity of force dipoles

$$\langle\Delta m^2\rangle_A = \langle\Delta m^2\rangle - \langle\Delta m^2\rangle_{eq}. \tag{19}$$

Because $\langle\Delta m^2\rangle = C(0)$, we have

$$\langle\Delta m^2\rangle_A = \frac{w_0}{w_0 + w_1}\left(k_1\ell_1^2 - k_0\ell_0^2\right)k_B T. \tag{20}$$

As follows from Eq. (17), the equilibrium fluctuation intensity is

$$\langle\Delta m^2\rangle_{eq} = k_0\ell_0^2 k_B T + 2(k_B T)^2. \tag{21}$$

Since the effective binding rate w_0 of the substrate is proportional to its concentration c, i.e., $w_0 = \eta c$, Eq. (20) yields the Michaelis-Menten form of the dependence of $\langle\Delta m^2\rangle_A$ on the substrate concentration.

Remarkably, the catalytic activity of the model enzyme can thus lead not only to some enhancement, but also to *reduction* of fluctuations of the force dipoles. According to Eq. (20), reduction should be observed if $k_1\ell_1^2 < k_0\ell_0^2$. Under this condition, the ligand-bound dimer ($s = 1$) is characterized by a lower fluctuation intensity of force dipoles than the free dimer ($s = 0$).

B. The limit of $w_0\tau_0 \gg 1$ and $w_0\tau_0 \gg 1$

In the limit characterized by conditions $w_0\tau_0 \gg 1$ and $w_0\tau_0 \gg 1$, transitions take place once the respective transitions windows are entered. If additionally the conditions $k_0\ell_0^2 \gg k_B T$ and $k_1\ell_1^2 \gg k_B T$ are satisfied, thermal fluctuations can be neglected and the dimer essentially behaves as a deterministic oscillator.

Then, the solution can be obtained by integrating Eq. (5) with appropriate boundary conditions. This yields $x(t) = \ell_1 + (\ell_0 - \ell_1 - \rho)e^{-t/\tau_1}$ for $0 < t < T_1$ and $x(t) = \ell_0 + (\ell_1 - \ell_0 + \rho)e^{-(t-T_1)/\tau_0}$ for $T_1 < t < T_c$. Here, T_c is the oscillation period of the active dimer and T_1 is the duration of the cycle time when the dimer is in the ligand-bound state $s = 1$. If transition windows are narrow, i.e., the condition $\rho \ll (\ell_0 - \ell_1)$ is satisfied, we approximately have

$$T_1 = \tau_1 \ln\left(\frac{\ell_0 - \ell_1}{\rho}\right), \tag{22}$$

and

$$T_{\rm c} = (\tau_0 + \tau_1) \ln\left(\frac{\ell_0 - \ell_1}{\rho}\right). \tag{23}$$

The respective time-dependent force dipole is $m(t) = k_1(\ell_1 - x)x$ for $0 < t < T_1$ and $m(t) = k_0(\ell_0 - x)x$ for $T_1 < t < T_{\rm c}$. Hence, it is negative for $s = 1$ and positive for $s = 0$.

The force dipole varies within the interval $m_{\rm min} < m < m_{\rm max}$, where the minimum value $m_{\rm min} = -k_1\ell_0(\ell_0 - \ell_1)$ is taken at $t = 0$, i.e., in the state $s = 1$ just after substrate binding, and the maximum value $m_{\rm max} = k_0\ell_1(\ell_0 - \ell_1)$ is reached at $t = T_1$, in the state $s = 0$ just after product release (here we again assume that transition windows are narrow). Note that, if thermal fluctuations were present, the force dipoles could however have also taken the values outside of this interval.

It can be checked by direct integration that the period-averaged force dipole for the deterministic active dimer is $\langle m(t)\rangle_{\rm det} = 0$. The correlation function for the deterministic oscillating dimer is defined as the period average

$$C_{\rm det}(t) = \frac{1}{T_{\rm c}} \int_0^{T_{\rm c}} dh\, m(t + h)m(h). \tag{24}$$

It is a periodic function on time.

The mean-square intensity of force dipoles is $\langle m(t)^2\rangle_{\rm det} = C_{\rm det}(0)$. In the limit $\rho \to 0$, we approximately have

$$\langle m(t)^2\rangle_{\rm det} = \frac{k_0 k_1}{12(k_0 + k_1)} \left[\ln\left(\frac{\ell_0 - \ell_1}{\rho}\right)\right]^{-1} (\ell_0 - \ell_1)^2$$
$$\times \left[k_0(\ell_0^2 + 2\ell_0\ell_1 + 3\ell_1^2) + k_1(3\ell_0^2 + 2\ell_0\ell_1 + \ell_1^2)\right]. \tag{25}$$

When $k_1 \sim k_0$, this equation yields the scaling $\langle m(t)^2\rangle_{\rm det} \sim k_0^2$.

C. The limit of $w_0\tau_0 \ll 1$ and $w_1\tau_1 \gg 1$

If the conditions $w_0\tau_0 \ll 1$ and $w_1\tau_1 \gg 1$ are satisfied, the model enzyme waits a long time for binding of a substrate (because the substrate concentration is low), but then it performs a rapid reaction cycle. An approximate solution in this regime can be obtained if, additionally, the conditions $k_0\ell_0^2 \gg k_{\rm B}T$ and $k_1\ell_1^2 \gg k_{\rm B}T$ are satisfied, i.e., that thermal fluctuations are weak. Moreover, we shall assume that the transition window for substrate binding is narrow, i.e., the approximation (9) holds for $u_0(x)$.

In this case, the dependence $x(t)$ consists of a sum of statistically independent rare pulses, each corresponding to one reaction cycle:

$$x(t) = \sum_j z(t - t_j), \tag{26}$$

where $z(t) = \ell_1 + (\ell_0 - \ell_1)e^{-t/\tau_1}$ for $0 < t < T_1$ and $z(t) = \ell_0 + (\ell_1 - \ell_0)e^{-(t - T_1)/\tau_0}$ for $t > T_1$, with T_1 given by Eq. (22). The pulses appear at random time moments t_j and the probability of their appearance per unit time is w_0.

Moreover, we also have

$$m(t) = \sum_j \zeta(t - t_j), \tag{27}$$

where $\zeta(t) = k_1(\ell_1 - z(t))z(t)$ for $0 < t < T_1$ and $\zeta(t) = k_0(\ell_0 - z(t))z(t)$ for $t > T_1$.

Hence, this represents a random Poisson process. Its first two statistical moments are approximately $\langle m(t)\rangle = 0$ and

$$\langle m^2(t)\rangle = w_0 \int_0^\infty dt\, \zeta^2(t) = \frac{1}{12}w_0\tau_0(\ell_0 - \ell_1)^2$$
$$\times \left[k_0^2(\ell_0^2 + 2\ell_0\ell_1 + 3\ell_1^2) + k_0 k_1(3\ell_0^2 + 2\ell_0\ell_1 + \ell_1^2)\right]. \tag{28}$$

Taking into account Eq. (11), it can be noticed that, when $k_1 \sim k_0$, the scaling $\langle m^2(t)\rangle \sim k_0^{3/2}$ should hold.

D. The limit of $w_0\tau_0 \gg 1$ and $w_1\tau_1 \ll 1$

Finally, the situation with $w_0\tau_0 \gg 1$ and $w_1\tau_1 \ll 1$ corresponds to substrate saturation and a long waiting time for the reaction and product release in the ligand-bound state. A derivation, similar to that given above, shows that, if $k_0\ell_0^2 \gg k_{\rm B}T$ and $k_1\ell_1^2 \gg k_{\rm B}T$, we approximately have $\langle m(t)\rangle = 0$ and

$$\langle m^2(t)\rangle = \frac{1}{12}w_1\tau_1(\ell_0 - \ell_1)^2$$
$$\times \left[k_1^2(3\ell_0^2 + 2\ell_0\ell_1 + \ell_1^2) + k_0 k_1(\ell_0^2 + 2\ell_0\ell_1 + 3\ell_1^2)\right]. \tag{29}$$

If we take into account Eq. (12), it can be noticed that, when $k_1 \sim k_0$, scaling $\langle m^2(t)\rangle \sim k_0^{3/2}$ is again obtained.

IV. NUMERICAL SIMULATIONS OF ACTIVE DIMERS

Before proceeding to simulations, the model was non-dimensionalized. The dimensionless variables were $\tilde{t} = t/\tau_0, \tilde{x} = x/\ell_0, \tilde{m} = m/(k_0\ell_0^2)$. The dimensionless transition rates were $\tilde{v}_0 = v_0\tau_0, \tilde{v}_1 = v_1\tau_0$ and the dimensionless temperature was $\theta = k_{\rm B}T/(k_0\ell_0^2)$. Stochastic differential equation (5) was numerically integrated, complemented by transitions between the ligand states.

In the simulations, we had $\ell_1 = 0.55\ell_0$, $k_1 = 2k_0$ and $\rho = 0.01\ell_0$. We have kept constant $\tilde{v}_1 = 2$, but varied the parameter $\tilde{v}_0$. Our intention was to numerically investigate statistical properties of the active dimer approaching
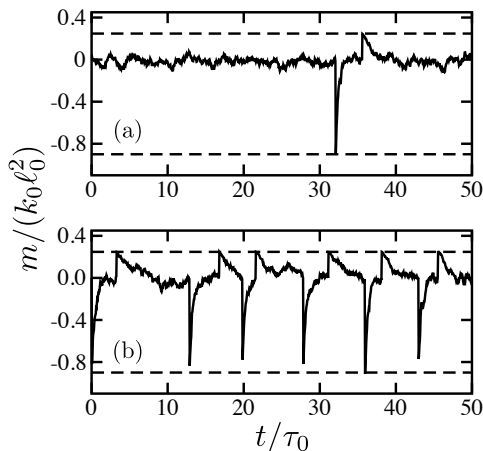
FIG. 3. Time dependence of dimensionless force dipoles $\widetilde{m} = m/(k_0\ell_0^2)$ on time for (a) $\tilde{v}_0 = 0.03$ and (b) $\tilde{v}_0 = 3$. Dashed lines show the lower bound $\widetilde{m}_{\min} = -0.9$ for the deterministic oscillatory dimer and the absolute upper bound $\widetilde{m}_{\max} = 0.25$ for force dipoles.

the deterministic regime. Therefore, a relatively low dimensionless temperature $\theta = 0.0018$ was chosen. Under such choice, $\langle m(t)^2 \rangle_{\text{det}}/\langle \Delta m^2 \rangle_{\text{eq}} = 19.3$ and $w_1\tau_1 = 0.27$.

Note that, because of the last condition, there was a significant random variation in the waiting times for substrate conversion and product release. Moreover, waiting times for substrate binding, characterized by the rate w_0, could also vary. These effects kept the model stochastic even when thermal noise was small.

Figure 3 shows typical time dependences of the force dipoles. In Fig. 3(a), the waiting time for substrate binding is long. Therefore, the dimer spends most of the time in the ligand-free state $s = 0$. Within the time shown, only one turnover cycle has taken place. For the force dipole, the cycle consists of a negative spike, just after binding of the substrate, and the following positive spike, just after the product release. In Fig. 3(b), the substrate binding rate is increased. As a result, the dimer is frequently cycling, already resembling an oscillator. Nonetheless, the random variation of the times between the cycles is relatively large.

Probability distributions of force dipoles are shown in Fig. 4. The black curve is the distribution for passive dimers in the absence of the substrate, given by Eq. (14). It represents a narrow Gaussian peak at $m = 0$. The distribution at $\tilde{v}_0 = v_0\tau_0 = 0.03$ (red) is almost indistinguishable from it. The blue curve is the distribution for active dimers corresponding to Fig. 3(b). Now, the distribution is more broad and the central peak is smaller. The tail on the left side from the peak and the shoulder on its right side are due to the non-equilibrium activity of force dipoles.

The dependence of the non-equilibrium part of the fluctuation intensity of force dipoles, Eq. (19), on the substrate binding rate v_0, proportional to substrate concentration, is shown in Fig. 5. It can be well fitted to the
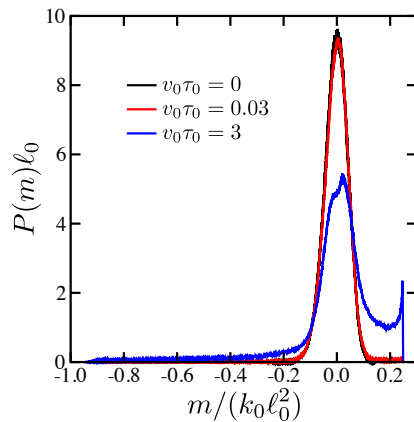

FIG. 4. Probability distributions of force dipoles $\widetilde{m}$ for passive (black curve, $v_0 = 0$) and active (red curve, $\tilde{v}_0 = 0.03$, and blue curve, $\tilde{v}_0 = 3$) dimers.
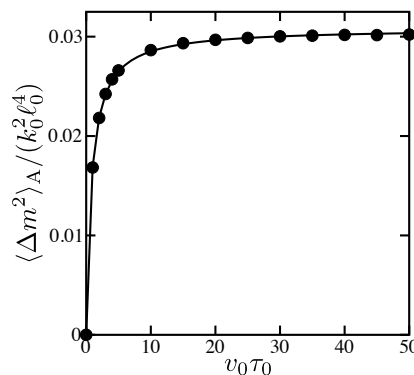

FIG. 5. Dependence of the non-equilibrium part $\langle \Delta m^2 \rangle_{\text{A}}$ of the fluctuation intensity of force dipoles on the substrate binding rate v_0 (dots). The solid curve is a fit to the Michaelis-Menten function.

Michaelis-Menten function (the solid curve). The saturation magnitude is close to the value of 0.033 predicted at such parameters for the deterministic dimer by Eq. (25).

Normalized correlation functions of force dipoles at different substrate binding rates are shown in Fig. 6. In the absence of the substrate (for $v_0 = 0$) the dependence is monotonous (it is given by Eq. (17)). As the substrate concentration is increased, damped oscillations in the correlation function become observed, thus signaling the onset of the active oscillatory behavior that prevails over the thermal noise.

The correlation functions could be fitted (dashed curves in Fig. 6) to the dependence

$$C(t)/C(0) = \frac{1}{\cos\alpha}\exp(-\Gamma|t|)\cos(\Omega|t| - \alpha). \quad (30)$$

Figure 7 shows how the dimensionless relaxation time $1/(\Gamma\tau_0)$, the dimensionless oscillation period $2\pi/(\Omega\tau_0)$ and the phase shift α depend on the substrate binding rate. The oscillation period under saturation conditions is still larger than $T_c/\tau_0 = 5.7$ for the deterministic dimer
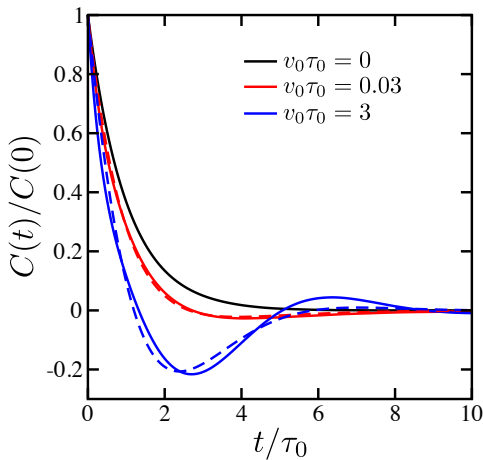
FIG. 6. Normalized correlation functions of force dipoles at different substrate binding rates: $v_0 = 0$ (absence of substrate, black), $\tilde{v}_0 = 0.03$ (red), and $\tilde{v}_0 = 3$ (blue). The correlation function for passive dimers (black) is given by Eq. (17). Dashed curves are fits to the dependence (30).
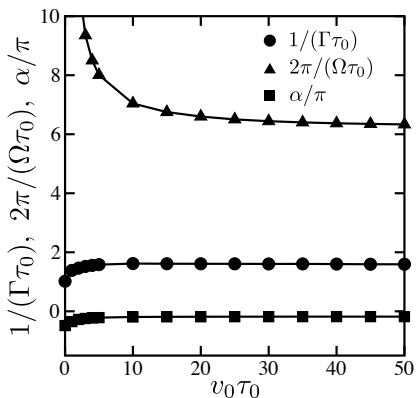

FIG. 7. The dependences of the relaxation time $1/\Gamma$ (circles), oscillation period $2\pi/\Omega$ (triangles) and phase shift α (squares) on substrate binding rate v_0.

according to Eq. (23). This is because of an additional waiting time for product release. The characteristic relaxation time is about $1/(\Gamma\tau_0) = 2$.

It should be stressed that the form (30) of the correlation function would not hold in the deterministic limit. Indeed, the oscillations stay harmonic in the limit of an infinite correlation time. However, the deterministic oscillations are actually non-harmonic, as seen in Fig. 3.

There are two effects that make the dimer model stochastic, i.e., the thermal noise in the dynamical equation (5) and random transitions between the ligand states $s = 0$ and $s = 1$. When $\theta \to 0$, the thermal noise vanishes, but random transitions between the states nonetheless remain. This second stochastic effect is responsible for the decay in the correlation function. As shown in Appendix C, the dependence of the correlation function in Eq. (30) corresponds to an approximate solution of the master equations (7) and (8).

V. DIFFUSION EFFECTS OF ENZYMES IN SOLUTION

The results of the previous two sections make it possible to obtain more accurate estimates for diffusion enhancement of passive particles in solutions of mechanochemically active enzymes.

The change D_A in the diffusion coefficient of passive *tracer* particles in a three-dimensional (3D) solution is given by [12, 14]

$$D_{\mathrm{A}} = \frac{n}{60\pi\mu^2\ell_{\mathrm{cut}}}(\chi - \chi_{\mathrm{eq}}). \tag{31}$$

Here, n is the concentration of active enzymes, μ is viscosity, ℓ_{cut} is a microscopic cut-off length and

$$\chi = \int_0^\infty dt\, C(t)\sigma(t), \tag{32}$$

where $C(t)$ is the correlation function of force dipoles corresponding to the enzymes and $\sigma(t)$ is the orientational correlation function for them. Moreover, χ_{eq} is the equilibrium part corresponding to $C(t) = C_{\mathrm{eq}}(t)$.

Thus, to estimate the magnitude of diffusion enhancement in solution, one needs to know the force-dipole correlation function $C(t)$ for the involved enzymes. In the original publication [12], it was assumed that this correlation function decays exponentially with the correlation time of the order of the turnover time of the considered enzymes. Moreover, the magnitude m of force dipoles was only roughly estimated, by using molecular motors as an example and taking $m = FL$ where L is the size of the motor protein and F is its stall force. It remained however not clear whether and to what extent such estimates would generally hold.

Furthermore, it was assumed [12] that orientations of force dipoles were randomly distributed, but remained frozen in time. While this assumption may indeed be satisfied, e.g., in the situations where enzymes are localized within a polymer matrix, rotational diffusion of such molecules has to be taken into account for water solutions of enzymes. Later on, rotational diffusion was taken into account and Eq. (31) was obtained [14]; nonetheless, in the analysis [14], it was assumed that the property χ was known for the considered enzymes.

Below, we obtain quantitative estimates for diffusion effects by using our results for model mechanochemical dimer enzymes.

Generally, the orientational correlation function can be approximated by an exponential form

$$\sigma(t) = \exp(-t/\tau_{\mathrm{rot}}), \tag{33}$$

where τ_{rot} is the orientational correlation time.

Orientational correlation times depend on the shape and size of proteins; they become increased in crowded solutions of them [24–26]. Nonetheless, they would never exceed a microsecond for typical enzymes.

On the other hand, the characteristic correlation time for force dipoles is determined by processes of slow conformational relaxation involving relative domain motions in such proteins. The time scales of such relaxation processes would typically lie in the microsecond to millisecond range. Since this is longer than $\tau_{\rm rot}$, the correlation function $C(t)$ of force dipoles would not typically change much within the orientational correlation time.

Below, we provide the estimates in the dimer model assuming that the orientational correlation time is much shorter than the correlation time for force dipoles. By using Eq. (33) and putting $C(t) \approx C(0) = \langle \Delta m^2 \rangle$ in Eq. (32), we find that approximately

$$\chi - \chi_{\rm eq} = \tau_{\rm rot} \langle \Delta m^2 \rangle_{\rm A}. \tag{34}$$

Hence, the change in the diffusion coefficient can be estimated as

$$D_{\rm A} = \frac{\tau_{\rm rot} n}{60 \pi \mu^2 \ell_{\rm cut}} \langle \Delta m^2 \rangle_{\rm A}. \tag{35}$$

This equation relates the magnitude of the diffusion change $D_{\rm A}$ to the non-equilibrium part $\langle \Delta m^2 \rangle_{\rm A}$ of the fluctuation intensity for hydrodynamical force dipoles of enzymes.

First, we consider the limit $w_0 \tau_0 \ll 1$ and $w_1 \tau_1 \ll 1$. This holds when the model dimer enzyme has to wait for a long time for binding of a substrate (because the substrate binding rate w_0 is proportional to substrate concentration c and this concentration is small). Moreover, there is also a long waiting time for the product formation (and release). Using Eq. (20), we find that, in this kinetic regime,

$$D_{\rm A} = \frac{\tau_{\rm rot} w_0 n}{60 \pi \mu^2 \ell_{\rm cut} (w_0 + w_1)} \left(k_1 \ell_1^2 - k_0 \ell_0^2 \right) k_{\rm B} T. \tag{36}$$

According to this result, not only diffusion enhancement, but also diffusion *reduction* can be caused by active enzymes. The latter takes place if the condition $k_1 \ell_1^2 < k_0 \ell_0^2$ is satisfied. In this case, the intensity of force dipoles in the ligand-bound state is smaller than in the ligand-free state.

Our numerical simulations at different substrate concentrations c (i.e., at different substrate binding rates w_0 proportional to c) have shown the Michaelis-Menten concentration dependence of $\langle \Delta m^2 \rangle_{\rm A}$ (see Fig. 5). This agrees with the analytical results in Sec. III, where we have found that $\langle \Delta m^2 \rangle_{\rm A}$ is proportional to w_0 at low concentrations [cf. Eqs. (20) and (28)], whereas it becomes saturated at high substrate concentrations [cf. Eqs. (25) and (29)]. As follows from Eq. (35), a Michaelis-Menten dependence on the substrate concentration should then hold also for a change in the diffusion coefficient $D_{\rm A}$. Such concentration dependence of $D_{\rm A}$ was conjectured in the previous study [12].

The maximum diffusion enhancement effect can thus be expected under the substrate saturation condition and if, additionally, there is no long waiting time for product formation and its release, i.e., in the limit of $w_0 \tau_0 \gg 1$ and $w_0 \tau_0 \gg 1$ in the subsection B in Sec. III. We can use the results for this limit to estimate the maximum magnitude of such effect and also to determine the conditions under which it would be strong.

The maximum possible intensity for force dipoles is then given by Eq. (25). Taking into account that sizes ℓ_0 and ℓ_1 of an enzyme in its two ligand states cannot differ much and also that the two stiffness constants k_0 and $k_1 = k_0 + \kappa$ cannot be largely different, this equation can be approximately written as

$$\langle m^2 \rangle_{\rm det} \approx \zeta_0 k_0^2 \ell_0^2 (\ell_0 - \ell_1)^2, \tag{37}$$

where ζ_0 is a dimensionless factor of order unity that also includes the logarithmic term. Note that this result corresponds to the deterministic limit when thermal fluctuations are vanishingly small. Therefore, we have $\langle \Delta m^2 \rangle_{\rm A,max} \approx \langle m^2 \rangle_{\rm det}$.

An important property of an enzyme is the energy ΔE supplied to it and dissipated in mechanochemical motions in each turnover cycle. For considered active dimers, it is given by Eq. (10).

Suppose that the energy ΔE is fixed. Then, using Eq. (10), we can determine the respective change in the dipole length as

$$\ell_0 - \ell_1 = \sqrt{\frac{2 \Delta E}{k_0 + k_1}}. \tag{38}$$

Substituting this into Eq. (37), a simple estimate can be obtained:

$$\langle \Delta m^2 \rangle_{\rm A,max} = \zeta_1 k_0 \ell_0^2 \Delta E, \tag{39}$$

where ζ_1 is another dimensionless factor of order unity.

Substituting this into Eq. (35), we find

$$D_{\rm A,max} = \frac{\zeta_1 \tau_{\rm rot} n k_0 \ell_0^2 \Delta E}{60 \pi \mu^2 \ell_{\rm cut}}. \tag{40}$$

Thus, the magnitude of diffusion enhancement under substrate saturation conditions is proportional to the energy ΔE supplied to an enzyme and dissipated by it within each turnover cycle.

According to the Stokes equation, rotational diffusion coefficient for a spherical particle of radius R is

$$D_{\rm rot} = \frac{k_{\rm B} T}{8 \pi \mu R^3}. \tag{41}$$

The orientational correlation time is $\tau_{\rm rot} = 1/D_{\rm rot}$. Note that, since proteins are not spheres, but have more complex shapes, their rotational times are shorter by up an order of magnitude than given by this. To approximately estimate $\tau_{\rm rot} = 1/D_{\rm rot}$ for the dimers, we nonetheless use this expression with $R = \ell_0$, but shall keep in mind that this overestimates the actual orientational correlation time.

The equilibrium diffusion constant for spherical tracer particles of radius R_0 is

$$D_T = \frac{k_B T}{6\pi\mu R_0}. \tag{42}$$

Here, we choose [13] the microscopic cut-off length as $\ell_{cut} = \ell_0 + R_0$.

Substituting this into Eqs. (35) and (37), we find

$$\frac{D_{A,max}}{D_T} = \nu\left(\frac{\Delta E}{k_B T}\right)\left(\frac{k_0\ell_0^2}{k_B T}\right)\left(\frac{\ell_0}{\ell}\right)^3\left(\frac{R_0}{R_0+\ell_0}\right), \tag{43}$$

where $\nu = 4\pi\zeta_1/5$ is a numerical factor of order unity and $\ell = n^{-1/3}$ is the mean distance in the solution between two neighboring enzymes.

According to Eq. (43), the relative diffusion enhancement gets larger for more exothermic enzymes, i.e., with the higher energy ΔE dissipated within a turnover cycle. It also increases for more stiff enzymes, characterized by a larger stiffness constant k_0 of the link connecting the two domains. Moreover, the diffusion enhancement for passive tracer particles is proportional to concentration of the enzymes. Finally, the magnitude of relative diffusion enhancement depends on the size R_0 of the passive particles, but this dependence becomes saturated for the probe particles larger than the enzyme.

For numerical estimates, we consider exothermic stiff enzymes with $\Delta E = 10k_B T$ and $k_0\ell_0^2 = 10k_B T$. Then, the mean square-root intensity $\langle\langle\Delta m^2\rangle_{A,max}\rangle^{1/2}$ of active force dipole, given by Eq. (39), is about 10^{-19} N·m. This is about ten times larger than the previous estimate [12] based on the stall forces for typical molecular motors.

As the enzyme concentration, we take $n = 1\,\mu M$. This corresponds to a non-crowded solution where the mean distance between the enzymes is about ten times larger than their size ($\ell \sim 10\ell_0$). Moreover, we consider passive particles with the sizes comparable to that of an enzyme ($R_0 \sim \ell_0$). As follows from Eq. (43), under these conditions, the change $D_{A,max}$ in the diffusion constant of such tracer particles can be of the same order of magnitude as the thermal diffusion constant D_T for them. At higher enzyme concentrations, approaching the crowded situation, the non-equilibrium diffusion enhancement may even dominate over thermal diffusion for passive particles of a protein size.

At the end of this section, we briefly discuss how the diffusion enhancement would generally depend on the orientational correlational time τ_{rot}, not assuming that it is much shorter than the correlation time for force dipoles. If the approximation in Eq. (30) holds, diffusion enhancement is determined by Eq. (31) where χ is given by Eq. (D1) in Appendix D. The diffusion enhancement depends non-monotonously on the orientational correlation time. It increases linearly with τ_{rot} at short times, then reaches a maximum at $\tau_{rot} = (\Omega - \Gamma)^{-1}$ and finally saturates at large orientational correlation times.

For example, if we take the values $\Gamma \approx 1/(2\tau_0)$ and $\Omega \approx \pi/(3\tau_0)$ corresponding to substrate saturation in

Fig. 7, the maximum diffusion enhancement would be reached at $\tau_{rot} = 1.8\tau_0$ and, at the maximum, it will be larger by about 30 percent than in the limit $\tau_{rot} \gg \tau_0$.

VI. DIFFUSION EFFECTS OF ACTIVE PROTEIN INCLUSIONS IN BIOMEMBRANES

It is known that, on the length scales shorter than the Saffman-Delbrück length of about a micrometer, lipid bilayers behave as 2D fluids [8]. Similar to enzymes in water solutions, active protein inclusions (such as ion pumps or transporters) can cyclically change their shapes inside a lipid bilayer within each ligand turnover cycle. Hence, they behave as hydrodynamical force dipoles within a fluid lipid bilayer. Therefore, diffusion enhancement is expected [12] for biomembranes when non-equilibrium conformational activity of proteins takes place.

A significant difference to water solution is that, for the biomembranes as 2D fluids, hydrodynamic diffusion enhancement effects are non-local. For such systems, Eq. (31) is replaced by [12, 14]

$$D_{A,\alpha\alpha'}(\mathbf{R}) = \frac{1}{32\pi^2\mu_{2D}^2}(\chi - \chi_{eq})\int d\mathbf{r}\,\frac{r_\alpha r_{\alpha'}}{r^4}n_{2D}(\mathbf{R}+\mathbf{r}). \tag{44}$$

Here, χ is again given by Eq. (32) with $\sigma(t)$ being the planar orientational correlation function for protein inclusions. Moreover, μ_{2D} is the 2D viscosity of the lipid bilayer, related as $\mu_{2D} = h\mu_{3D}$ to its 3D viscosity μ_{3D} (where h is the bilayer thickness); n_{2D} is the 2D concentration of active inclusions within the membrane.

For numerical estimates, we assume that active proteins occupy a small circular region (a raft) of radius R_m (shorter than the Saffman-Delbrück length) within a membrane. Then, diffusion enhancement for a passive particle of radius R_0 located in the center of the disc is [12, 14]

$$D_A = \zeta_m\frac{n_{2D}}{\mu_{2D}^2}(\chi - \chi_{eq}), \tag{45}$$

where $\zeta_m = (1/32\pi)\ln(R_m/\ell_{cut})$, $\ell_{cut} = R_0 + \ell_0$, and χ is given by the integral in Eq. (32) where, however, $\sigma(t)$ is the planar orientational correlation function for proteins inside a membrane.

The viscosity μ_{3D} of lipid bilayers is about 10^3 times higher than that of water and, therefore, both translational and rotational diffusion is much slower in them. From experiments, it is known that diffusion constants for proteins in lipid bilayers are about $D_T = 10^{-10}$ cm^2/s, i.e., about 10^3 times smaller than in water for similar proteins. One can therefore expect that rotational diffusion of proteins in lipid bilayers would be slowed by about a factor of 10^3 too, yielding orientational correlation times τ_{rot} that might approach a millisecond.

On the other hand, in contrast to solution enzymes that can be fast, with the turnover times of about $10\,\mu s$

for, e.g., urease, cycle times of active protein inclusions in biomembranes would typically be of the order of ten milliseconds. Therefore, they are still longer than the orientational correlation times. This means that Eq. (34) shall still approximately hold.

The magnitude of diffusion enhancement in Eq. (45) can be determined by modeling protein inclusions as active dimers that lie flat in the membrane. Then, the same estimates for $\langle \Delta m^2 \rangle_A$ as above can be used. Combining all terms, diffusion enhancement in Eq. (45) for a passive particle in the center of a protein raft approximately is

$$D_A = \nu_m \tau_{\rm rot} \left(\frac{k_B T}{h \ell_{\rm 2D} \mu_{\rm 3D}} \right)^2 \left(\frac{\Delta E}{k_B T} \right) \left(\frac{k_0 \ell_0^2}{k_B T} \right), \quad (46)$$

where the dimensionless prefactor is $\nu_m = \zeta_1 \zeta_m$ and $\ell_{\rm 2D} = n_{\rm 2D}^{-1/2}$ is the mean distance between inclusions in the membrane.

To obtain a numerical estimate, the 3D viscosity of the lipid bilayer is chosen as $\mu_{\rm 3D} = 1$ Pa·s and the thickness of the bilayer as $h = 1$ nm. For protein inclusions, we assume that $\Delta E = 10\, k_B T$ and $k_0 \ell_0^2 = 10\, k_B T$. The orientational correlation time is taken to be $\tau_{\rm rot} = 100\, \mu$s and the mean lateral distance between the proteins is $\ell_{\rm 2D} = 10$ nm. For such parameter values, the maximal possible diffusion enhancement under substrate saturation conditions is about $D_A = 10^{-9}\, {\rm cm}^2/{\rm s}$. For comparison, Brownian diffusion constants for proteins in lipid bilayers are of the order of $10^{-10}\, {\rm cm}^2/{\rm s}$ and diffusion constants for lipids are about $10^{-8}\, {\rm cm}^2/{\rm s}$.

VII. ANALYSIS OF EXPERIMENTAL DATA

Diffusion enhancement has been reported in solutions of several catalytically active enzymes, at the concentrations varying between 1 nM and 10 nM [27–31]. With the exception of aldolase [30] (for which, however, the enhancement could not be independently confirmed [32]), all these enzymes were exothermic and had high turnover rates of about $10^4\, {\rm s}^{-1}$. The enhancement was reported not only for the enzymes themselves, but also for inert molecules (tracers) in solutions of them [27, 28]. The enzyme concentration dependence of the diffusion enhancement effects could *not* however be detected [29].

It does not seem plausible that such experimental data can be understood in the framework of the original theory [12] and its subsequent extensions, including the present work. The fact that a significant diffusion enhancement (by tens of percent) was observed already at low nanomole concentrations can still be perhaps explained by assuming that, for some reasons, the force dipoles of specific enzymes with high catalytic turnover rates were exceptionally strong. However, the absence of a dependence of the experimentally observed diffusion enhancement on the enzyme concentration clearly contradicts the theory [12] where diffusion enhancement arises as a collective hydrodynamic effect.

Experiments on optical tracking of particles in animal cells [33] and in bacteria or yeast [34] have been furthermore performed. They have shown that, when metabolism was suppressed (by depletion of ATP), diffusion dropped to undetectable levels [33, 35] or it was much slowed down and replaced by subdiffusion characteristic for a colloidal glass [34]. Strong reduction of diffusion under metabolism suppression was moreover found in various cytoplasm extracts [36].

It should be also noted that diffusion enhancement has been experimentally observed within chromatin in a living biological cell [37]. This was explained by active operation of molecular machines involved in transcription and translation of DNA [38].

The cytoplasm of a living cell represents a crowded solution of proteins. In bacteria, the volume fraction of proteins in cytosol is about 30 percent [39], with the highest concentrations of the order of $100\, \mu$M reached for glycolysis enzymes. Most of the enzymes in the cell are mechanochemical, i.e., they exhibit conformational changes in their catalytic cycles. Typical turnover times of enzymes in a biological cell are of the order of 10 ms.

According to the previous [12] and current estimates, substantial diffusion enhancement due to hydrodynamic collective effects should thus be expected under metabolism in the cytoplasm. There are, however, also other mechanisms that can contribute to diffusion enhancement in the cells.

The cytoskeleton of animal cells represents an active gel, with numerous myosin molecular motors operating within it. It is known that the activity of the motors can lead to development of non-equilibrium fluctuations in the cytoskeleton which induce in turn fluctuations and diffusion enhancement in the cytosol [17, 35, 40]. The skeleton of bacteria and yeast is however passive; moreover, metabolic diffusion enhancement in such cells could also be observed when their skeleton was chemically resolved [34]. Therefore, the active gel mechanism [40] cannot account for the effects observed in them.

On the other hand, under high crowding characteristic for cytoplasm, proteins are frequently colliding and direct interactions between them often take place [24, 26]. It is known that, for dense colloids, glass behavior can be expected, with the transport and relaxation phenomena strongly slowed down in them [41]. Indeed, such behavior could be observed both in the cells [34] and in the extracts [36] in the absence of metabolism.

It has been recently shown that, when the particles forming a glass-like colloid, cyclically change their shapes, the colloid gets fluidized and classical transport properties become restored [42, 43]. Even in the absence of hydrodynamic interactions, conformational activity of proteins, at the rates of energy supply of about $10\, k_B T$ per a protein molecule per a cycle, can lead to diffusion enhancement by one order of magnitude [42]. This provides an additional, non-hydrodynamic, mechanism that can contribute to the experimentally observed diffusion enhancement in living biological cells.

VIII.   ANALYSIS OF COMPUTATIONAL DATA

Large-scale computer simulations for colloids of active dimers have been performed by Dennison, Kapral and Stark [20]. In these simulations, the solvent was explicitly included and the multiparticle collision dynamics (MPCD) approximation [22] was employed, thus allowing to fully account for hydrodynamic effects.

To facilitate the comparison, we first give a summary of the essential parameter values in the study [20], using the current notations employed by us. The natural lengths of the dimer in two ligand states were ℓ_0 and $\ell_1 = \ell_0/2$, and the spring constants were k_0 and $k_1 = 2k_0$. The dimensionless spring constant $k\ell_0^2/k_BT$, characterizing stiffness of the dimer, was varied between 144 and 1440. The energy $\Delta E = (1/2)(k_0 + k_1)(\ell_0 - \ell_1)^2$, supplied to a dimer and dissipated by it as heat within a single cycle, was changing therefore between $121.5\,k_BT$ and $1215\,k_BT$. The simulations were performed under substrate saturation conditions. Product formation and release were possible within a window of half-width $\rho = 0.025\ell_0$ near $x = \ell_1$. The rate v_1 of this transition could be varied in the simulations by a factor of 5.

The Langevin equation (5) with viscous friction and thermal noise was not used. Instead, collisions between the two beads of the dimer and the solvent particles were explicitly taken into account in the framework of MPCD. For a single passive dimer, the equilibrium correlation function of force dipoles $C_{eq}(t)$ was computed yielding the correlation time for fluctuations of its force dipole; this function could be well fitted to the theoretical dependence in Eq. (17). Note that, when $k_0\ell_0^2/k_BT \gg 1$, the relaxation time $\tau_0 = (\gamma k_0)^{-1}$ of the dimer should be close to this correlation time. Moreover, we have $\tau_1 = (\gamma k_1)^{-1} = \tau_0/2$. Using such estimates, it can be shown that $w_1\tau_1$ varied between 0.001 and 0.1 in the simulations [20]. Because substrate saturation was assumed, conditions $w_0\tau_0 \gg 1$ and $w_1\tau_1 \ll 1$ corresponding to the limit D in Sec. III were therefore approximately satisfied.

For single active dimers, correlation functions $C(t)$ of force dipoles were determined [20]. They showed damped oscillations and were similar to the correlation function for $v_0\tau_0 = 3$ in Fig. 6. The correlation times varied, but remained of the same order of magnitude as the correlation time of the passive dimer. The force-dipole intensity $\langle \Delta m^2 \rangle$ of active dimers was by about an order of magnitude larger than $\langle \Delta m^2 \rangle_{eq}$ for the passive ones. Depending on the parameters, it scaled as k_0^α with the exponent α in the range between 1.2 and 1.6, comparable with the exponent of 1.5 in Eq. (29).

Orientational correlation functions $\sigma(t)$ were furthermore computed for single dimers [20]. Remarkably, it was found that the orientational correlation time τ_{rot} was sensitive to the conformational activity of the dimer, getting shorter by about an order of magnitude when such activity was switched on. Nonetheless, in all simulations τ_{rot} was larger than the force dipole correlation time.

Multiparticle 3D computer simulations of colloids formed by active dimers were further performed [20]. In the simulations, the truncated potential

$$u(r) = 4\epsilon \left[\left(\frac{2r_0}{r} \right)^{48} - \left(\frac{2a}{r_0} \right)^{24} + \frac{1}{4} \right], \qquad (47)$$

for $r < 2^{1/24}(2r_0)$ and zero otherwise, with $\epsilon = 2.5\,k_BT$ and $r_0 = 1.075\ell_0$, was used to describe steep repulsive interactions between the beads belonging to different dimers. The interaction radius r_0 was chosen as defining the radius of a bead.

Since distances ℓ_0 and $\ell_1 = 0.5\ell_0$ in the open and closed dimer conformations were both smaller than $2r_0 = 2.15\ell_0$, large overlaps between the beads in a dimer were present in the simulations. However, this did not affect the internal dimer dynamics because there were no repulsive interactions between the beads in the same dimer. Additionally, the simulated system included one passive tracer particle of radius $0.5\ell_0$.

The volume fraction ϕ occupied by dimers was determined by taking into account the overlaps, but assuming that all dimers were in the equilibrium open state with the length of ℓ_0. Because, under substrate saturation conditions, they were however mainly found in the closed state with an even stronger overlap, such definition overestimated the actual volume fraction by a factor of up to two.

Due to the crowding effects, diffusion of a passive particle in the system of inactive dimers decreased with the volume fraction of them. The diffusion reduction at the highest taken volume fraction $\phi = 0.266$ was less than ten percent, indicating that this colloidal system was still far from the glass transition threshold [41].

When the dimers were active, diffusion of tracers was increasing instead with the dimer volume fraction ϕ. For the most stiff active dimers with $k_0\ell_0^2/k_BT = 1440$ and the kinetic regime with $w_1\tau_1$ about 0.1, relative diffusion enhancement of $D_A/D_T = 0.3$ could be observed [20] at the dimer volume fraction of $\phi = 0.266$. For the least stiff dimers with $k_0\ell_0^2/k_BT = 144$, diffusion enhancement by 5 percent was seen at $\phi = 0.133$.

Thus, collective hydrodynamic effects of active enzymes on diffusion of passive particles could be computationally confirmed. To speed up the calculations, model enzymes in the study [20] were chosen however to be unusually rapid (with the turnover times shorter than the rotational diffusion time) and unusually exothermic (with the heat release of hundreds of k_BT per a turnover cycle). It would be therefore important to undertake such simulations also for the parameters closer approaching those of the real enzymes.

IX.   DISCUSSION

By using the minimal active dimer model as an example, we have analytically and numerically investigated hydrodynamic effects of mechanochemical enzymes. The

intensity and other statistical properties of their force dipoles have been thus considered in different kinetic regimes. Thus, detailed estimates for diffusion enhancement in solutions of catalytically active enzymes under the conditions of fast rotational diffusion have been obtained. As we have found, higher diffusion enhancement should be expected for more strongly exothermic enzymes with more rapid mechanochemical motions associated with their turnover cycles.

Based on these results, currently available experimental and computational data has been examined. We have concluded that, while the collective hydrodynamic effects of diffusion enhancement have been principally confirmed in the computational study [20], further work is needed to bring simulations closer to the parameter region corresponding to real enzymes.

On the experimental side, we have concluded that the data on diffusion enhancement in weak nanomole solutions of several fast exothermic enzymes cannot be explained in the framework of the theory [12] and alternative explanations for them should be sought. In experimental studies of diffusion phenomena in living cells and in cellular extracts, additional work is needed to distinguish possible hydrodynamic contributions from the effects of direct collisions between active proteins and the resulting kinetic crowding effects. Large-scale numerical simulations of crowded active colloids including hydrodynamic interactions between the particles are to be performed.

Finally, we point out that, although the effects of diffusion enhancement are also predicted for biomembranes crowded with active protein inclusions, experiments and numerical multiparticle simulations of such phenomena are still missing today. It would be interesting and important to carry out them.

Appendix A

When transitions between the states $s = 0$ and $s = 1$ are rare, the solution of the master equations (7) and (8) can be approximately sought in the form

$$p_s(x, t) = \pi_s(t) p(x, t|s), \qquad (A1)$$

where $\pi_s(t)$ is the probability to find the dimer in the ligand state s and $p(x, t|s)$ is the probability distribution for distance x provided that the dimer is (permanently) in the state s.

Substituting these expressions into Eqs. (7) and (8) and integrating over the variable x, one finds that the probabilities π_s obey classical master equations for a two-level system,

$$\frac{d\pi_0}{dt} = w_1 \pi_1 - w_0 \pi_0, \qquad (A2)$$

and

$$\frac{d\pi_1}{dt} = w_0 \pi_0 - w_1 \pi_1. \qquad (A3)$$

Here w_0 and w_1 are effective rates of transitions between the states given by

$$w_0 = \int_{-\infty}^{\infty} dx\, u_0(x) p(x|s = 0), \qquad (A4)$$

and

$$w_1 = \int_{-\infty}^{\infty} dx\, u_1(x) p(x|s = 1). \qquad (A5)$$

The involved probability distributions in the statistically stationary case are

$$p(x|s = 0) = \sqrt{\frac{k_0}{2\pi k_B T}} \exp\left[-\frac{k_0}{2k_B T}(x - \ell_0)^2\right], \quad (A6)$$

and

$$p(x|s = 1) = \sqrt{\frac{k_1}{2\pi k_B T}} \exp\left[-\frac{k_1}{2k_B T}(x - \ell_1)^2\right]. \quad (A7)$$

If the transition windows are narrow, approximations (9) can furthermore be used, so that we obtain

$$w_0 = \nu_0 p(x = \ell_0|s = 0), \qquad w_1 = \nu_1 p(x = \ell_1|s = 1). \tag{A8}$$

Thus, using the above expressions for distance distributions, we finally get

$$w_0 = 2\rho v_0 \sqrt{\frac{k_0}{2\pi k_B T}}, \qquad (A9)$$

and

$$w_1 = 2\rho v_1 \sqrt{\frac{k_1}{2\pi k_B T}}. \qquad (A10)$$

In the steady state, the probabilities are

$$\pi_0 = \frac{w_1}{w_0 + w_1}, \qquad \pi_1 = \frac{w_0}{w_0 + w_1}. \qquad (A11)$$

Appendix B

Let us consider the second statistical moment $\langle x^2 \rangle$. In a steady state, its time derivative is zero. On the other hand, by using Eqs. (7)–(8) and integrating by parts, we find

$$
\begin{aligned}
\frac{d\langle x^2 \rangle}{dt} \\
= 2\gamma \int_{-\infty}^{\infty} dx \left[k_0 x(\ell_0 - x) p_0(x) + k_1 x(\ell_1 - x) p_1(x) \right] \\
+ 2\gamma k_{\mathrm{B}} T \int_{-\infty}^{\infty} dx \left[p_0(x) + p_1(x) \right] \\
= 2\gamma \langle m \rangle + 2\gamma k_{\mathrm{B}} T = 0.
\end{aligned}
\tag{B1}
$$

Thus, we straightforwardly obtain that, for an active dimer in any statistically steady state, $\langle m \rangle = -k_{\mathrm{B}} T$.

Note that here and also in the equations below, the integration limits over x are taken as $+\infty$ and $-\infty$. The actual limits are automatically selected by probability distributions $p_0(x)$ and $p_1(x)$.

Appendix C

Introducing

$$
\mathbf{p}(x, t) = \begin{pmatrix} p_0(x, t) \\ p_1(x, t) \end{pmatrix},
\tag{C1}
$$

we can write the system of two master equations (7) and (8) concisely as

$$
\frac{d\mathbf{p}}{dt} = -\hat{\mathbf{L}} \mathbf{p},
\tag{C2}
$$

where

$$
\hat{\mathbf{L}} = \begin{pmatrix} \hat{L}_{00} & \hat{L}_{01} \\ \hat{L}_{10} & \hat{L}_{11} \end{pmatrix},
\tag{C3}
$$

and

$$
\hat{L}_{00} = \gamma k_0 \frac{\partial}{\partial x} (\ell_0 - x) - \gamma k_{\mathrm{B}} T \frac{\partial^2}{\partial x^2} + u_0(x),
\tag{C4}
$$

and

$$
\hat{L}_{11} = \gamma k_1 \frac{\partial}{\partial x} (\ell_1 - x) - \gamma k_{\mathrm{B}} T \frac{\partial^2}{\partial x^2} + u_1(x),
\tag{C5}
$$

and

$$
\hat{L}_{01} = -u_1(x), \qquad \hat{L}_{10} = -u_0(x).
\tag{C6}
$$

The general solution of Eq. (C2) is

$$
p_s(x, t) = \sum_{n=0}^{\infty} A_n q_s^{(n)}(x) e^{-\lambda_n t} + \text{c.c.}
\tag{C7}
$$

where λ_n and $\mathbf{q}^{(n)}$ are eigenvalues and eigenvectors of the linear operator $\hat{\mathbf{L}}$,

$$
\hat{\mathbf{L}} \mathbf{q}^{(n)} = \lambda_n \mathbf{q}^{(n)},
\tag{C8}
$$

and decomposition coefficients A_n are determined by initial conditions.

Because the master equation must have a stable stationary solution, the operator $\hat{\mathbf{L}}$ should always possess a zero eigenvalue $\lambda_0 = 0$ and, furthermore, condition $\mathrm{Re}\,\lambda_n > 0$ should hold for all other eigenvalues n (cf. [44]). Generally, the eigenvectors can be ordered according to the increase of $\mathrm{Re}\,\lambda_n$ (and therefore we can enumerate the eigenvalues in such a way that $0 < \mathrm{Re}\,\lambda_1 \leq \mathrm{Re}\,\lambda_2 \leq \mathrm{Re}\,\lambda_3 \leq ...$). The stationary probability distribution $\bar{\mathbf{p}}(x)$ coincides with the eigenvector $\mathbf{q}^{(0)}(x)$.

The conditional probability $G(x, s, t|x_0, s_0)$ gives the probability to find the dimer in various states (x, s) at time t provided that it was in the state (x_0, s_0) at time $t = 0$. It represents a special solution of the master equation (C2) given by

$$
G(x, s, t|x_0, s_0) = \sum_{n=0}^{\infty} a_n(x_0, s_0) q_s^{(n)}(x) e^{-\lambda_n t} + \text{c.c.}
\tag{C9}
$$

where $a_n(x_0, s_0)$ are the coefficients of decomposition of this initial condition over eigenvectors $\mathbf{q}^{(n)}$.

The force dipole m depends on the distance x between the domains and on the dimer state s, i.e., $m(t) = m(x(t), s(t))$. Therefore, in the statistically stationary state we have

$$
\begin{aligned}
\langle m(t) m(0) \rangle = \sum_{s, s_0 = 0, 1} \int_{-\infty}^{\infty} dx_0 \int_{-\infty}^{\infty} dx \, m(x_0, s_0) m(x, s) \\
\times \bar{p}_{s_0}(x_0) G(x, s, t|x_0, s_0).
\end{aligned}
\tag{C10}
$$

By using Eqs. (C9) and (C10), we find that, in the statistically stationary state, the correlation function of force dipoles is

$$
C(t) = \langle m(t) m(0) \rangle - \langle m^2 \rangle = \sum_{n=1}^{\infty} B_n e^{-\lambda_n |t|} + \text{c.c.}
\tag{C11}
$$

where the complex coefficients B_n are

$$
\begin{aligned}
B_n = \sum_{s, s_0 = 0, 1} \int_{-\infty}^{\infty} dx_0 \int_{-\infty}^{\infty} dx \, m(x_0, s_0) m(x, s) \\
\times \bar{p}_{s_0}(x_0) a_n(x_0, s_0) q_s^{(n)}(x).
\end{aligned}
\tag{C12}
$$

If we retain in this decomposition only the first, most slowly decaying term, this yields

$$
C(t) \approx B_1 e^{-\lambda_1 |t|} + \text{c.c.} = \frac{C(0)}{\cos \alpha} e^{-\Gamma |t|} \cos(\Omega |t| - \alpha).
\tag{C13}
$$

Therefore, the normalized correlation function is

$$\frac{C(t)}{C(0)} = \frac{1}{\cos\alpha}e^{-\Gamma|t|}\cos(\Omega|t|-\alpha), \qquad \text{(C14)}$$

where $\Gamma = \mathrm{Re}\,\lambda_1$, $\Omega = \mathrm{Im}\,\lambda_1$, and $B_1 = C(0)e^{i\alpha}/\cos\alpha$.

Our numerical simulations, described in Sec. IV, have shown that, in the regimes approaching a deterministic oscillatory dimer, the correlation functions of force dipoles could be well fitted to the above dependence. This suggests that contributions from the higher, more rapidly decaying relaxation modes $n > 1$ have been indeed relatively small. As generally known [45], noisy oscillators possess a slowly relaxing mode that corresponds to diffusion of the oscillation phase. It can be expected that, under chosen conditions, such a mode has been dominating the correlation functions for oscillatory dimers.

Appendix D

Suppose that the force-dipole correlation function $C(t)$ and the orientational correlation function $\sigma(t)$ are given by Eqs. (C14) and (33). By taking the integral in Eq. (32), we find

$$\chi = \frac{1/\tau_{\mathrm{rot}} + \Gamma + \Omega\tan\alpha}{(1/\tau_{\mathrm{rot}} + \Gamma)^2 + \Omega^2}\langle\Delta m^2\rangle. \qquad \text{(D1)}$$

This yields a non-monotonous dependence of χ on the orientational correlation time. If the phase shift α is small and can be neglected (cf. Fig. 7), the maximum value χ_{max} is reached at $\tau_{\mathrm{rot}} = (\Omega - \Gamma)^{-1}$ and we have

$$\frac{\chi_{\mathrm{max}}}{\chi_\infty} = \frac{\Gamma^2 + \Omega^2}{2\Gamma\Omega}, \qquad \text{(D2)}$$

where

$$\chi_\infty = \frac{\Gamma}{\Gamma^2 + \Omega^2}\langle\Delta m^2\rangle, \qquad \text{(D3)}$$

is the limit of χ when $\tau_{\mathrm{rot}} \gg \Gamma^{-1}$ and $\tau_{\mathrm{rot}} \gg \Omega^{-1}$.

[1] A. Cressman, Y. Togashi, A. S. Mikhailov, and R. Kapral, *Phys. Rev. E* **77**, 050901 (2008).
[2] C. Echeverria, Y. Togashi, A. S. Mikhailov, and R. Kapral, *Phys. Chem. Chem. Phys.* **13**, 10527 (2011).
[3] R. Golestanian and A. Ajdari, *Phys. Rev. Lett.* **100**, 038101 (2008).
[4] R. Golestanian and A. Ajdari, *J. Phys.: Cond. Matt.* **21**, 204104 (2009).
[5] M. Iima and A. S. Mikhailov, *EPL* **85**, 44001 (2009).
[6] T. Sakaue, R. Kapral, and A. S. Mikhailov, *Eur. Phys. J. B* **75**, 381 (2010).
[7] X. Bai and P. Wolynes, *J. Chem. Phys.* **143**, 165101 (2015).
[8] H. Diamant, *J. Phys. Soc. Jpn.* **78**, 041002 (2009).
[9] M.-J. Huang, A. S. Mikhailov, R. Kapral, and H.-Y. Chen, *J. Chem. Phys.* **137**, 055101 (2012).
[10] M.-J. Huang, A. S. Mikhailov, R. Kapral, and H.-Y. Chen, *J. Chem. Phys.* **138**, 195101 (2013).
[11] M.-J. Huang, H.-Y. Chen, and A. S. Mikhailov, *Eur. Phys. J. E* **35**, 119 (2012).
[12] A. S. Mikhailov and R. Kapral, *Proc. Natl. Acad. Sci. USA* **112**, E3639 (2015).
[13] R. Kapral and A. S. Mikhailov, *Physica D* **318-319**, 104 (2016).
[14] A. S. Mikhailov, Y. Koyano, and H. Kitahata, *J. Phys. Soc. Jpn.* **86**, 101013 (2017).
[15] Y. Koyano, H. Kitahata, and A. S. Mikhailov, *Phys. Rev. E* **94**, 022416 (2016).
[16] Y. Hosaka, K. Yasuda, R. Okamoto, and S. Komura, *Phys. Rev. E* **95**, 052407 (2017).
[17] K. Yasuda, R. Okamoto, S. Komura, and A. S. Mikhailov, *EPL* **117**, 38001 (2017).
[18] K. Yasuda, R. Okamoto, and S. Komura, *Phys. Rev. E* **95**, 032417 (2017).
[19] Y. Hosaka, S. Komura, and D. Andelman, *Phys. Rev. E* **101**, 012610 (2020).
[20] M. Dennison, R. Kapral, and H. Stark, *Soft Matter* **13**, 3741 (2017).
[21] F. Kogler, Interactions of artificial molecular machines. Diploma Thesis (Technical University of Berlin, 2012).
[22] R. Kapral, *Adv. Chem. Phys.* **140**, 89 (2008).
[23] H. Flechsig and A. S. Mikhailov, *J. Roy. Soc. Interface* **16**, 20190244 (2019).
[24] S. von Bülow, M. Siggel, M. Linke, and G. Hummer, *Proc. Natl. Acad. Sci. USA* **116**, 9843 (2019).
[25] Z. Bashardanesh, J. Elf, H. Zhang, and D. van der Spoel, *ACS Omega* **4**, 20654 (2019).
[26] G. Nawrocki, A. Karaboga, Y. Sugita, and M. Feig, *Phys. Chem. Chem. Phys.* **21**, 876 (2019).
[27] K. K. Dey, *Angew. Chem. Int. Ed.* **58**, 2208 (2019).
[28] A.-Y. Jee, S. Dutta, Y.-K. Cho, T. Tlusty, and S. Granick, *Proc. Natl. Acad. Sci. USA* **115**, 14 (2018).
[29] M. Xu, J. L. Ross, L. Valdez, and A. Sen, *Phys. Rev. Lett.* **123**, 128101 (2019).
[30] P. Illien, X. Zhao, K. Dey, P. J. Butler, A. Sen, and R. Golestanian, *Nano Lett.* **17**, 4415 (2017).
[31] C. Riedel, R. Gabizon, C. A. M. Wilson, K.Hamadani, K. Tsekouras, S. Marqusee, S. Presse, and C. Bustamante, *Nature* **517**, 227 (2015).
[32] Y. Zhang, M. J. Armstrong, N. M. B. Kazeruni, and H. Hess, *Nano Lett.* **18**, 8025 (2018).
[33] M. Guo, A. J. Ehrlicher, M. H. Jensen, M. Renz, J. R. Moore, R. D. Goldman, J. Lippincott-Schwartz, F. C. MacKintosh, and D. A. Weitz, *Cell* **158**, 822 (2014).
[34] B. R. Parry, I. V. Surovtsev, M. T. Cabeen, C. S. O'Hem, E. R. Dufresne, and C. Jacobs-Wagner, *Cell* **156**, 183 (2014).

[35] E. Fodor, M. Guo, N. S. Gov, P. Visco, D. A. Weitz, and F. van Wijland, *EPL* **110**, 48005 (2015).

[36] K. Nishizawa, K. Fujiwara, N. Ikenaga, N. Nakajo, and D. Mizuno, *Sci. Rep.* **7**, 15143 (2017).

[37] S. C. Weber, A. J. Spakowitz, and J. A. Theriot, *Proc. Natl. Acad. Sci. USA* **109**, 7338 (2012).

[38] R. Bruinsma, A. Y. Grosberg, Y. Rabin, and A. Zidovska, *Biophys. J* **106**, 1871 (2014).

[39] A. Vendeville, D. Lariviere, and E. Fourmentin, *FEMS Microbiol. Rev.* **35**, 395 (2010).

[40] F. C. MacKintosh and A. J. Levine, *Phys. Rev. Lett.* **100**, 018104 (2008).

[41] G. L. Hunter and E. R. Weeks, *Rep. Prog. Phys.* **75**, 066501 (2012).

[42] Y. Koyano, H. Kitahata, and A. S. Mikhailov, *EPL* **128**, 40003 (2019).

[43] N. Oyama, T. Kawasaki, H. Mizuno, and A. Ikeda, *Phys. Rev. Research* **1**, 032038 (2019).

[44] H. Risken, *The Fokker-Planck Equation: Methods of Solution and Applications* (Springer, Berlin 1989).

[45] Y. Kuramoto, *Chemical Oscillations, Waves and Turbulence* (Springer, Berlin 1984).